BAMS Article

Meteosat Third Generation (MTG)

Continuation and Innovation of Observations from Geostationary Orbit

K. Holmlund, J. Grandell, J. Schmetz, R. Stuhlmann, B. Bojkov, R. Munro, M. Lekouara, D. Coppens, B. Viticchie, T. August, B. Theodore, P. Watts, M. Dobber, G. Fowler, S. Bojinski, A. Schmid, K. Salonen, S. Tjemkes, D. Aminou, and P. Blythe

ABSTRACT: Within the next couple of years, the European Organisation for the Exploitation of Meteorological Satellites (EUMETSAT) will start the deployment of its next-generation geostationary meteorological satellites. The Meteosat Third Generation (MTG) is composed of four imaging (MTG-I) and two sounding (MTG-S) platforms. The satellites are three-axis stabilized, unlike the two previous generations of Meteosat that were spin stabilized, and carry two sets of remote sensing instruments each. Hence, in addition to providing continuity, the new system will provide an unprecedented capability from geostationary orbit. The payload on the MTG-I satellites are the 16-channel Flexible Combined Imager (FCI) and the Lightning Imager (LI). The payloads on the MTG-S satellites are the hyperspectral Infrared Sounder (IRS) and a high-resolution Ultraviolet–Visible–Near-Infrared (UVN) sounder Sentinel-4/UVN, provided by the European Commission. Today, hyperspectral sounding from geostationary orbit is provided by the Chinese *Fengyun-4A* (*FY-4A*) satellite Geostationary Interferometric Infrared Sounder (GIIRS) instrument, and lightning mappers are available on *FY-4A* and on the National Oceanic and Atmospheric Administration (NOAA) *GOES-16* and *GOES-17* satellites. Consequently, the development of science and applications for these types of instruments have a solid foundation. However, the IRS, LI, and Sentinel-4/UVN are a challenging first for Europe in a geostationary orbit. The four MTG-I and two MTG-S satellites are designed to provide 20 and 15.5 years of operational service, respectively. The launch of the first MTG-I is expected at the end of 2022 and the first MTG-S roughly a year later. This article describes the four instruments, outlines products and services, and addresses the evolution of the further applications.

KEYWORDS: Atmosphere; Lightning; Satellite observations; Soundings; Nowcasting; Atmospheric composition

https://doi.org/10.1175/BAMS-D-19-0304.1
Corresponding author: K. Holmlund, work4ken@gmail.com
In final form 18 December 2020

AFFILIATIONS: Holmlund, Grandell, Schmetz, Stuhlmann, Bojkov, Munro, Lekouara, Coppens, Viticchie, August, Theodore, Watts, Dobber, Fowler, Bojinski, and Schmid—European Organisation for the Exploitation of Meteorological Satellites, Darmstadt, Germany; **Salonen**—European Centre for Medium Range Weather Forecasts, Reading, United Kingdom; **Tjemkes**—Atmospheric and Environmental Research Division, Verisk Analytics GmbH, Munich, Germany; **Aminou and Blythe**—European Space Technology Centre, European Space Agency, Noordwijk, Netherlands

The Meteosat Third Generation (MTG) program will bring the European imagery capabilities to the current state of the art with the new Flexible Combined Imager (FCI). In addition, the MTG satellites will fly three different Earth observation instruments, marking a major improvement over previous geostationary meteorological satellite systems. The FCI and the Lightning Imager (LI) will share one platform, the so-called MTG imager platform (MTG-I). The Infrared Sounder (IRS), an interferometer, and the high-resolution Ultraviolet–Visible–Near-Infrared (UVN) spectrometer Sentinel-4/UVN of the Copernicus Programme (www.copernicus.eu/en) are hosted on the second so-called sounding platform (MTG-S). Figure 1 shows the two MTG satellite types with the two Earth observation instruments on each platform. The MTG fleet comprises in total six satellites, four MTG-I and two MTG-S satellites, providing long-term continuity with 20 and 15.5 years of operational service, respectively. While spin-stabilized satellites have been highly successful, they only view the Earth a fraction of the time. This poses limitations to the emitted radiance available for the instruments. Furthermore, the novel instruments, like the Lightning Imager, would not be realistic to deploy. The MTG satellites will therefore be three-axis stabilized, unlike the two previous Meteosat generations, which were spin stabilized. The transition to a three-axis stabilized system is necessary in order to meet the stringent requirements not only for the FCI, but also for LI, IRS, and Sentinel-4/UVN.

The MTG program dates back to 2000, when EUMETSAT and the European Space Agency (ESA) initiated joint preparatory activities toward the definition of a MTG geostationary system, starting with a formal user consultation process, ensuring continuity and improvement over the current geostationary Meteosat Second Generation (MSG) satellites, which have been flown since 2002 (e.g., Schmetz et al. 2002). The primary MSG payload, the 12-channel SEVIRI (Spinning Enhanced Visible and Infrared Imager), was the benchmark for geostationary imagery for 15 years until the launch of the Advanced Himawari Imager (AHI) on *Himawari-8* in October 2014 (Bessho et al. 2015) by the Japan Meteorological Agency (JMA) and followed by the launches of AHI/*Himawari-9* in November 2016 and the National Oceanic and Atmospheric Administration (NOAA) Advanced Baseline Imager (ABI) on *GOES-16* and *GOES-17* (Goodman et al. 2012) in November 2016 and March 2018 by the United States. AHI and ABI are the first instruments of the new-generation geostationary imagers with 16 channels, full-disk scanning every 10 min, and additional regional rapid scan capabilities (Schmit et al. 2017).

The MTG data and products generated within the EUMETSAT application ground segment will be made available in near–real time through delivery mechanisms like EUMETCast and the World Meteorological Organization (WMO) Global Telecommunication System

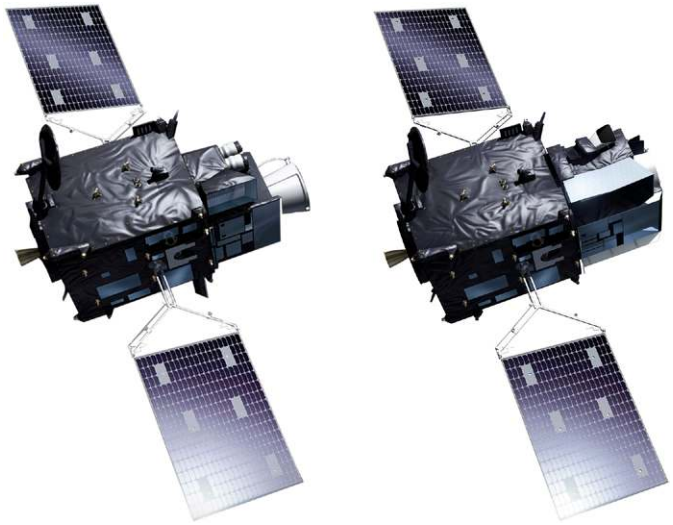

Fig. 1. The MTG satellites: (left) MTG-I and (right) MTG-S. The two spacecraft are based on the same platform and bus with identical solar panels.

(GTS). Some of the high-data-rate, near-real-time dissemination may also be based on a terrestrial high-speed communication network. The offline and time series data and products will be available through the EUMETSAT Data Centre.

A previous summary of the MTG mission was published in *La Meteorologie* (Stuhlmann et al. 2017), but this *BAMS* article includes critical updates. The article is organized as follows. The second section describes the instruments and their products, while the third section focuses on the applications, including, for example, nowcasting and numerical weather prediction, monitoring hazards, and atmospheric composition. The fourth section discusses the additional benefits brought by MTG, and the final section concludes the article.

The MTG instruments and their products

Flexible Combined Imager. The FCI instrument will continue the successful mission of the SEVIRI instrument on MSG. The FCI has additional channels and improved spatial, temporal, and radiometric performance, compared to the current SEVIRI. The requirements for the FCI are driven by regional and global numerical weather prediction (NWP) and nowcasting. The FCI design allows a Full-Disk Scan Service (FDSS), with a basic repeat cycle of 10 min, and an alternative fixed European regional Rapid-Scan Service (RSS), which covers one-quarter of the full disk with a repeat cycle of 2.5 min. It is planned to provide this dual capability once two MTG-I satellites have been successfully deployed, with one satellite dedicated to FDSS and one to RSS.

Figure 2 provides a summary of the growth of imaging capabilities from the Meteosat First Generation (MFG) through the Second to the Third Generation. It shows how the spectral capabilities have increased while retaining the capabilities of the previous generation. The inserted squares depict in a comparative manner the improved spatial resolution at subsatellite point. The corresponding temporal repeat cycles for full-disk imaging for the three Meteosat generations are 30, 15, and 10 min, respectively. It should be noted that for the first three MFG satellites (*Meteosat-1–3*), visible channel data at 2.5-km resolution were not, due to limited downlink capabilities, available continuously and then only by omitting the water vapor channel data (de Waard et al. 1992). Furthermore, the MSG SEVIRI instrument includes a high-resolution broadband visible channel at 1-km resolution, but only covering half of the visible disk in the east–west direction (e.g., Schmetz et al. 2002).

The FDSS scans the full Earth disk with a revisit time of 10 min and a spatial resolution of 1 km (at the subsatellite point) for eight solar spectrum channels and 2-km resolution for eight infrared channels. The 3.80-μm channel is realized with two radiometric ranges, one from 200 to 350 K and one from 350 to 450 K. The latter enables better detection and quantitative analysis of fire temperatures. For the RSS the data from FCI are provided on regional scales (e.g., 1/4 of the full disk as seen from the geostationary position) at a refresh rate of about 2.5 min. Four of the FCI channels are available on ground at a double resolution of 0.5 km (0.64 and 2.25 μm) and 1.0 km (3.80 and 10.50 μm). These high-resolution products are available for both full disk and the rapid scanning local area. The key specifications of FCI are given in Table 1. Note that the central wavelengths provided in Table 1 are the specified ones and the actual ones will be marginally different.

FCI will provide continuity in observing atmospheric parameters established by the previous-generation Meteosat satellites, but also improved capabilities in terms of products and accuracy in legacy products. Some of the improvements FCI brings include improved aerosol retrieval contributing to air-quality monitoring; total water vapor retrieval during daytime over land using the 0.9-μm channel, thus helping nowcasting applications; cloud analysis improved with the 1.3-μm channel for thin cirrus detection; and cloud microphysics, which will be enhanced during daytime, resolving smaller-scale variations in convective updrafts due to the higher spatial resolution. The advanced monitoring of clouds from FCI

	Meteosat 1st Generation			Meteosat 2nd Generation			Meteosat 3rd Generation		
Core channels	Central wavelength micron	Width (FWHM) micron	Spatial Sampling (km)	Central wavelength micron	Width (FWHM) micron	Spatial Sampling (km)	Central wavelength micron	Width (FWHM) micron	Spatial Sampling (km)
VIS 0.4							0.444	0.06	1.0
VIS 0.5							0.510	0.05	1.0
VIS 0.6	0.7	0.35	2.5	0.635	0.08	3.0	0.640	0.08	0.5
VIS 0.8				0.81	0.07	3.0	0.865	0.07	1.0
VIS 0.9							0.914	0.06	1.0
NIR 1.3							1.380	0.03	1.0
NIR 1.6				1.64	0.14	3.0	1.610	0.06	1.0
NIR 2.2							2.250	0.05	0.5
IR 3.8				3.9	0.44	3.0	3.800	0.40	1.0
IR.6,3	6.1	1.3	5.0	6.2	1.0	3.0	6.300	1.00	2.0
IR 7.3				7.35	0.5	3.0	7.350	0.50	2.0
IR 8.7				8.7	0.4	3.0	8.700	0.40	2.0
IR 9.7				9.66	0.3	3.0	9.660	0.30	2.0
IR 10.5	11.5	1.9	5.0	10.8	1.0	3.0	10.500	0.7	1.0
IR 12.3				12.0	1.0	3.0	12.300	0.50	2.0
IR13.3				13.4	1.0	3.0	13.300	0.60	2.0
Repeat cycle	30 min			15 min			10 min		

Fig. 2. The growth of imaging capabilities for the Meteosat satellites. The inserted squares depict in a comparative manner the improved spatial resolution at subsatellite point. The corresponding temporal repeat cycles for full-disk imaging for the three Meteosat generations are 30, 15, and 10 min, respectively. The channel reference is the MTG FCI Core channels (FC). Finally, all Meteosat satellites can be operated in a rapid-scan mode, covering a certain portion of the disk at higher temporal resolution.

will also benefit from the additional observations from the IRS, as noted by Mecikalski et al. (2011), in particular for better all-day (including the night) cloud microphysical properties. More generally, substantial improvements in monitoring the mesoscale environment can be expected through the combined use of FCI and IRS (e.g., Schmit et al. 2009), and exploiting the shorter repeat cycle and better spatial resolution of FCI. A key product derived from geostationary imagery data is atmospheric motion vectors (AMVs). AMVs are wind observations derived by tracking cloud or water-vapor features in consecutive satellite images, and the increased spatial and temporal resolution provided by FCI will also enable the derivation of higher-density AMVs for NWP. In addition to these parameters, additional benefits from the combined use of FCI and IRS can be expected for a wide range of applications, including trace gases/air quality, dust detection, and climate (Schmit at al. 2009). Table 2 gives an overview of the main benefits of the FCI channels for various atmospheric parameters.

The observations of the above parameters are provided in a set of baseline products. The committed EUMETSAT Level 2 products from the FCI available at the start of operations are presented in Table 3.

Table 1. The key specification of the Flexible Combined Imager on board MTG. Note that the central wavelengths provided are the specified ones and the actual ones will be marginally different.

MTG imagery band	Central wavelength (μm)	Spectral width (μm)	Reference signal α_{ref} [a]	Radiometric noise (SNR)	Spatial sampling distance (SSD) (km)
VIS 0.4	0.444	0.060	0.01	>25	1.0
VIS 0.5	0.510	0.040	0.01	>25	1.0
VIS 0.6	0.640	0.050	0.01	>30–12[b]	1.0–0.5[b]
VIS 0.8	0.640	0.050	0.01	>30	1.0
VIS 0.8	0.865	0.050	0.01	>21	1.0
VIS 0.9	0.914	0.020	0.01	>12	1.0
NIR 1.3	1.380	0.030	0.01	>40	1.0
NIR 1.6	1.610	0.050	0.01	>30	1.0/0.5[b]
NIR 2.2	2.250	0.050	0.01	>25–12[b]	1.0–0.5[b]
			Reference signal T_{ref} (K)	**Radiometric noise (NEdT) (K)**	
IR 3.8	3.80	0.400	300	<0.1–0.2[b]	2.0–1.0[b]
			350	1[c]	
IR 6.3	6.30	1.00	250	<0.3	2.0
IR 7.3	7.35	0.50	250	<0.3	2.0
IR 8.7	8.70	0.40	300	<0.1	2.0
IR 9.7	9.66	0.30	250	<0.3	2.0
IR 10.5	10.5	0.70	300	<0.1–0.2[b]	2.0–1.0[b]
IR 12.3	12.3	0.50	300	<0.2	2.0
IR 13.3	13.3	0.60	270	<0.2	2.0

[a] The value α_{ref} represents the reflectance at the top of atmosphere (TOA) multiplied by the cosine of the solar zenith angle, i.e., $\alpha_{ref} = \rho\cos\theta_s$ allowing minimum, maximum, and reference signals in terms of spectral radiance at the TOA to be derived for the VNIR spectral channels.

[b] The spectral channels VIS 0.6, NIR 2.2, IR 3.8, and IR 10.5 are delivered in both Full Disk High Spectral Resolution Imagery (FDHSI) sampling and a High Resolution and Fast Imagery (HRFI) sampling configurations.

[c] For the IR 3.8 channel the dynamic range has been extended with a reduced radiometric noise specification for active fire monitoring.

With the launch of MTG-I FCI, the geostationary ring will, except for a part over the Indian Ocean, be fully covered by the extended capabilities of the new-generation geostationary imagers. Similar capabilities are, or will be, also available from the main meteorological polar-orbiting satellite systems provided by NOAA, the China Meteorological Administration (CMA), and EUMETSAT. This will enable opportunities for synergetic product development and provision of consistent state-of-the-art products across the full globe and will significantly enhance the overall capabilities of the meteorological satellite imagery capabilities. Table 4 presents a comparison of the current and foreseen new-generation geostationary and polar imagers.

Lightning Imager. The main objective of the LI mission is to detect, monitor, and track lightning for severe weather monitoring and lightning climatology and to provide, as a secondary objective, the potential for upper-tropospheric chemistry (NO_x production) monitoring (Grandell et al. 2010). The LI on MTG-I satellites will offer new observing capabilities primarily aimed at nowcasting but very interesting also for NWP and other applications. It will deliver near-real-time information on total lightning [intercloud (IC) and cloud to ground (CG)] for the full field of view. The continuous observations of total lightning are provided to users in quasi near–real time with a data latency on the order of 1 min. Together with the Geostationary Lightning Mapper (GLM) on NOAA *GOES-16/17* and later on GOES-T/U, and the Lightning

Table 2. The main capabilities of the FCI channels for various atmospheric parameters.

MTG imagery band	Central wavelength (μm)	Atmospheric parameter
VIS 0.4	0.444	Aerosol, volcanic ash
VIS 0.5	0.510	Aerosol, volcanic ash
VIS 0.6	0.640	Cloud detection and properties, AMV from cloud tracking, snow cover, vegetation, volcanic ash, smoke
VIS 0.8	0.865	Cloud detection and properties, AMV, cloud type, cloud phase, cloud optical depth, cloud microphysics, snow cover, vegetation stress, smoke detection, volcanic ash detection, volcanic ash concentration
VIS 0.9	0.914	Total column water vapor
NIR 1.3	1.380	Cirrus detection, water vapor
NIR 1.6	1.610	Cloud phase, cloud microphysics, cloud detection, cloud type, snow cover, vegetation stress, smoke detection
NIR 2.2	2.250	Cloud microphysics
IR 3.8	3.80	Cloud detection, cloud microphysics, sea surface and land surface temperature, fire[a]
IR 6.3	6.30	AMV from water vapor tracking, height assignment of tracers, instability and humidity monitoring
IR 7.3	7.35	AMV from water vapor tracking, instability and humidity monitoring
IR 8.7	8.70	Cloud detection, cloud type, cloud-top height, cloud microphysics, ash detection and high sulfur dioxide, sand/dust storm detection
IR 9.7	9.66	Total column ozone
IR 10.5	10.5	Cloud detection, AMV from cloud tracking, cloud type, cloud-top height, tracer heights, LST and SST, instability and humidity monitoring, volcanic ash and sand/dust
IR 12.3	12.3	Cloud detection, AMV from cloud tracking, height assignment of cloud tracers, instability and humidity monitoring, cloud total column humidity, SST and LST, volcanic ash and sand/dust
IR 13.3	13.3	Cloud-top height, atmospheric instability monitoring, volcanic ash detection

[a] There will be two IR3.8 L1c products (HRFI and FDHSI) merging the IR and the FA for a radiometric range covering 200 K to fire range.

Mapper Imager (LMI) on the Chinese Fengyun-4 (FY-4) satellite series (Yang et al. 2017), LI will establish a geostationary ring of lightning mappers.

The LI instrument has four optical heads, each one with a two-dimensional detector array providing a sample distance at the subsatellite point of 4.5 km and a baseline integration time of 1 ms (adjustable). The instrument measures the optical pulses at 777.4 nm using a 1.9-nm narrow bandpass filter. To detect risk areas related to lightning, information primarily on flashes and their density in space and time is required, but not necessarily information on individual strokes. The detection efficiency (DE) for the prime observable, the lightning optical pulses, is required to be better than 90% over central Europe and 70% over the full disk area observed by LI. We expect a decrease of the DE almost linearly with increasing distance from the subsatellite point (SSP). The flash DE is expected to be 90% and rather uniform within the field of view (FOV). A flash is linked to electrical discharges forming one or more strokes visible as optical pulses at cloud top. The analyzed statistics indicate that 90% of all flashes are linked with a stroke having at least one optical pulse of energy higher than 10 μJ m^{-2} sr^{-1}.

An important part of the LI is proper identification and filtering of noise and false detections caused by various artifacts, such as instrument microvibrations and energetic particles from surrounding space. During each integration timeframe, after removal of the background signal, the net signal for each pixel is compared to an adaptive threshold. The typical net optical pulse radiance will be above 4–7 μJ m^{-2} sr^{-1}, depending on the background brightness.

Table 3. The baseline MTG FCI product suite. TBC = to be confirmed.

Product generation processing chain	Product	Coverage	Resolution	Generation frequency	Dissemination	Format
FCI All-Sky Radiance	All-sky radiance	Full disk	32 × 32 VIS pixels 16 × 16 IR pixels	10 min	EUMETCast, RMDCN	BUFR, netCDF
FCI Clear-Sky Reflectance Map	Clear-sky reflectance map	Full disk	SW pixel	2 h between 0400 and 2000 UTC	EUMETCast	netCDF
FCI SCENE	Clear/cloud flag Dust storm detection Fire detection Volcanic ash	Full disk	IR pixel	10 min	EUMETCast, RMDCN	GRIB, CAP, netCDF
FCI OCA	Cloud optical thickness, top pressure, phase and effective radius for 1–2 layers	Full disk	IR pixel	10 min	EUMETCast	netCDF
FCI AMVs[a]	Atmospheric motion vectors	Full disk	Synoptic scale < 80 km	30 min	EUMETCast RMDCN	BUFR, netCDF
FCI GII	Global instability indices[b] Ozone–total column Specific humidity (SH) lower troposphere SH middle troposphere SH upper troposphere SH total column	Full disk	3 × 3 pixels	10 min	EUMETCast	netCDF
FCI Aerosols[c]	Aerosol (AER) asymmetry parameter AER optical depth–total column AER refractive index AER single scattering albedo AER size distribution	Full disk	SW pixel	3 h (TBC)	EUMETCast, RMDCN (TBC)	GRIB, netCDF

[a] AMV are extracted from the VIS0.8, IR3.8 (night only), WV6.3, WV7.3, and IR10.5 channels.
[b] The GII product contains two different indices.
[c] FCI aerosol products are not committed for day 1, but as aspirational product and all but aerosol optical depth (total column) are TBC.

The reduction of the total number of false transients through the Level 2 filtering is about three orders of magnitude during the day and two orders of magnitude at night, with the final Level 2 flash false alarm rate being on the order of a few false flashes per second per optical channel in the illuminated conditions and close to 0 in darkness. It should also be noted that there is some overlap in the areas covered by the four optical heads. Therefore, duplicate flashes will be removed as well as groups and events associated with the removed flashes. This will ensure the coherency of the event, group, and flash products. LI initial processing

Table 4. A comparison of the capabilities (central wavelength in micrometer) of the new-generation geostationary and polar imagers. In addition to those channels presented, *FY-3D*/MERSI-2 has the following channels in the visible and very/near-infrared: 0.470, 0.555, 0.936, 0.940 μm. RGB channels noted with red, green, and blue.

MTG channel	No.	MTG/FCI	*Himawari-8*/AHI	*GOES-16*/ABI	*KOMPSAT-2A*/AMI	*FY-4A*/AGRI	JPSS/VIIRS	*FY-3D*/MERSI-2	EPS-SG/MetImage
							0.412	0.412	
Blue	1	0.444			0.470		0.445	0.443	0.433
Blue			0.471	0.470		0.47	0.488	0.490	
Green	2	0.510	0.510		0.509		0.555	0.550	0.555
Red	3	0.640	0.639	0.637	0.639	0.65	0.640	0.650	
Red							0.672	0.670	0.668
							0.700	0.709	
4		0.865	0.857	0.864	0.863	0.825	0.746	0.746	0.752
									0.763
							0.865	0.865	0.865
5		0.914						0.905	0.914
							1.240	1.240	1.240
6		1.380		1.373	1.374	1.375	1.378	1.380	1.375
7		1.610	1.610	1.609	1.609	1.61	1.610	1.640	1.630
8		2.250	2.257	2.242		2.25	2.250	2.130	2.250
9		3.800	3.885	3.890	3.832	3.75	3.700	3.80	3.740
							3.740		3.959
							4.005	4.05	4.050
10		6.300	6.243	6.171	6.210	6.25			6.725
			6.941	6.927	6.941	7.1			
11		7.350	7.347	7.336	7.327			7.20	7.325
12		8.700	8.593	8.444	8.588	8.5	8.550	8.55	8.540
13		9.660	9.637	9.607	9.621				
14		10.500	10.407	10.331	10.354	10.7	10.763	10.80	10.690
			11.240	11.186	11.229	12.0	11.450		
15		12.300	12.381	12.266	12.365		12.013	12.00	12.020
16		13.300	13.281	13.266	13.287	13.5			13.345

is done on the nonrectified LI Level 1b detector grid. After duplicate flash removal, the accumulation is done by merging the accumulated products from the four Optical Channels over the FCI IR Level 1C 2-km grid. It should be noted that the current baseline is that the data will not be corrected for parallax effects, as the LI accumulated products are intended to be overlaid on FCI data for monitoring lightning activity in clouds. The retained and the triggered pixel measurements on the detector grid are called triggered events.

The key characteristics of LI are given in Table 5 and the coverage area is shown in Fig. 3.

Table 5. The key characteristics of the Lightning Imager on board MTG.

Measurement wavelength	777.4 nm
Coverage	84% of the disk observable from geostationary orbit (see Fig. 4)
Lightning detected	Cloud-to-cloud/intracloud (CC/IC) and cloud-to-ground (CG), without a separation of the types
Integration time per frame	1 ms
Ground sample distance at subsatellite point	4.5 km

The lightning events themselves, as recorded by the LI instrument, are not directly equivalent with geophysical lightning strokes, and clustering in space and time is needed to arrive at a product for end users. This is done in two steps: 1) pixel events are clustered into groups, which represent the measured optical pulses (and also lightning strokes), and 2) the groups are clustered into flashes. The adjacency in time and space is the most important group clustering criterion as optical pulses are continuous in time and space. A distinction between cloud-to-ground and cloud-to-cloud strokes is not pursued for the near-real-time products. The end-user products from the LI are divided into point products, also known as "initial processing" (flashes and groups) and accumulated (gridded, see below) products, where the data are cumulated over 30 s to provide a better overview of electrically active areas within the field of view. These 30-s datasets can be stacked by users for their application and visualization, e.g., a 10-min accumulation with a 30-s update frequency.

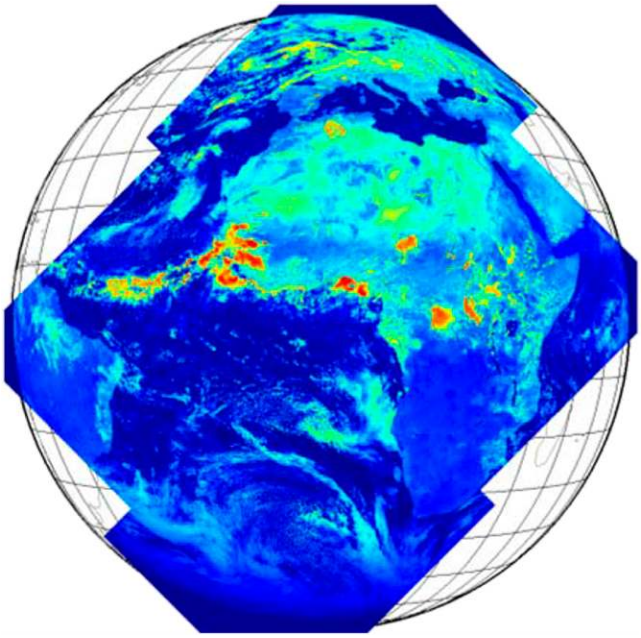

Fig. 3. MTG LI coverage showing the four identical detectors with small overlaps. The end-users will not see the detector structure but will get unified products without overlaps.

The committed products from the LI available at the start of operations are presented in Table 6. In addition to these products, novel applications, like using Level 0 and Level 1b data for the detection of bolides entering Earth's atmosphere, will be pursued in the future.

The Infrared Sounder. The IRS instrument on MTG-S is the first hyperspectral IR instrument on a geostationary satellite providing full-disk coverage. IRS will provide information on horizontally, vertically, and temporally (four-dimensional) resolved water vapor and temperature structures of the atmosphere. The IRS is based on an imaging Fourier-interferometer with a spectral resolution better than 0.754 cm^{-1} and a spectral sampling around 0.6 cm^{-1}. All interferograms from the IRS are disseminated (downlinked) to ground, where they are transformed into spectra via fast Fourier transformation and are radiometrically and spectrally calibrated and geolocated.

The IRS instrument takes measurements in two spectral bands: the longwave infrared (LWIR, 680–1210 cm^{-1} or 14.3–8.3 μm) with >800 spectral channels and the midwave infrared (MWIR, 1600–2250 cm^{-1} or 6.25–4.6 μm) with >920 channels, with a spatial resolution of

Table 6. The committed products from the LI instrument and distribution method. EUMETCast is the EUMETSAT legacy distribution method.

LI initial processing[a]	L2 lightning events[b]	LI pixel	10 s	Archive only	netCDF
	Lightning groups	LI pixel	10 s	EUMETCast	netCDF
	Lightning flash	LI pixel	10 s	EUMETCast	netCDF
LI accumulated products	Accumulated flash area	FCI IR pixel	30 s	EUMETCast	netCDF
	Accumulated flashes	FCI IR pixel	30 s	EUMETCast	netCDF
	Accumulated flash radiance	FCI IR pixel	30 s	EUMETCast	netCDF

[a] Of the products generated by the LI initial processing chain the L2 lightning events are not disseminated, but lightning groups and lightning flashes and the number of L2 lightning events contributing to the lightning groups are disseminated.

[b] From the initial processing, the lightning events product is not disseminated via EUMETCast, but available from the archive. The other initial processing products lightning groups and lightning flashes are disseminated via EUMETCast.

4 km at subsatellite point. The final number of channels will depend on the performance of the instrument. The spectral coverage of IRS will provide operational information of carbon monoxide and ozone as well as information about sulfur dioxide (e.g., from volcanic eruptions) and ammonia, all useful for air quality forecasts and atmospheric composition monitoring and thus complementing Sentinel-4/UVN observations. The observations are performed in a step-and-stare mode, in so-called dwells with a matrix detector of 160 × 160 pixels, ensuring contiguous hyperspectral imagery. The Earth disk is divided into four local area coverage (LAC) regions, which are each scanned within 15 min. The most northern quarter—comprising Europe—is referred to as LAC4 and is revisited every 30 min, interleaved with other disk quarters to cover a full disk according to a configurable scan pattern. The baseline scan pattern is given in Fig. 4.

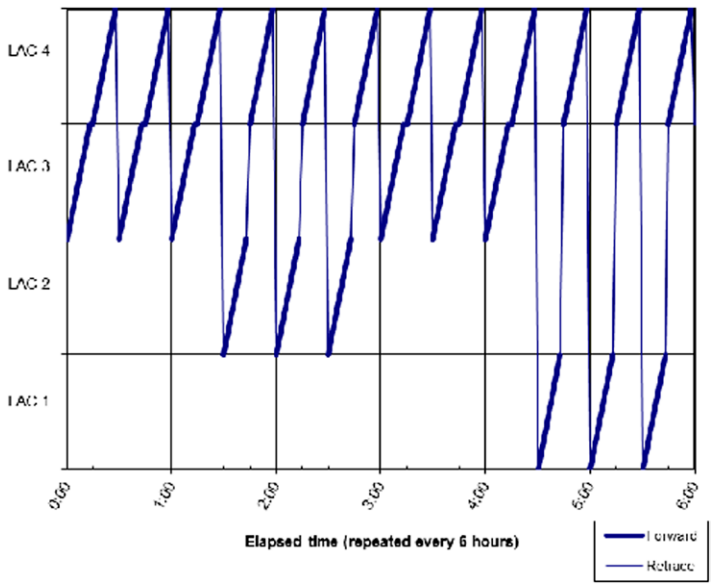

Fig. 4. The MTG IRS baseline scan pattern.

Figure 5 presents the scanned area of IRS and the actual corners for the upper quarter of the disk, and the key characteristics of IRS are given in Table 7.

Until recently, the only heritage for IRS has been interferometers on polar orbiters, for instance, the Infrared Atmospheric Sounding Interferometer (IASI) on MetOp (Klaes et al. 2007). Now CMA has launched the GIIRS instrument on *FY-4A* in December 2016 (Yang et al. 2017), and it has already provided valuable proxy data for the development of IRS products and applications enabling the development of mature algorithms for day 1. The main objective of the IRS is to provide information on specific humidity and temperature with good vertical resolution either via data assimilation methods or as retrieved profiles, which also drives the baseline scan sequence. The use of sequences of IRS data will also enable extracting information on atmospheric flow, either through the derivation of AMVs or via the wind tracing effect in four-dimensional variational (4D-Var) data assimilation schemes. Furthermore, IRS will be capable of providing trace gas information, and in addition to ozone and carbon monoxide profiles, there is some potential to derive carbon dioxide, ammonia (not as a profile but integrated quantity) (e.g., Warner et al. 2017), sulfur dioxide (in case of large quantities such as volcano eruptions), dust (index), and aerosol optical depth. In addition, there are many other potential uses of a high spectral IR sounder with high temporal measurements (Schmit et al. 2009).

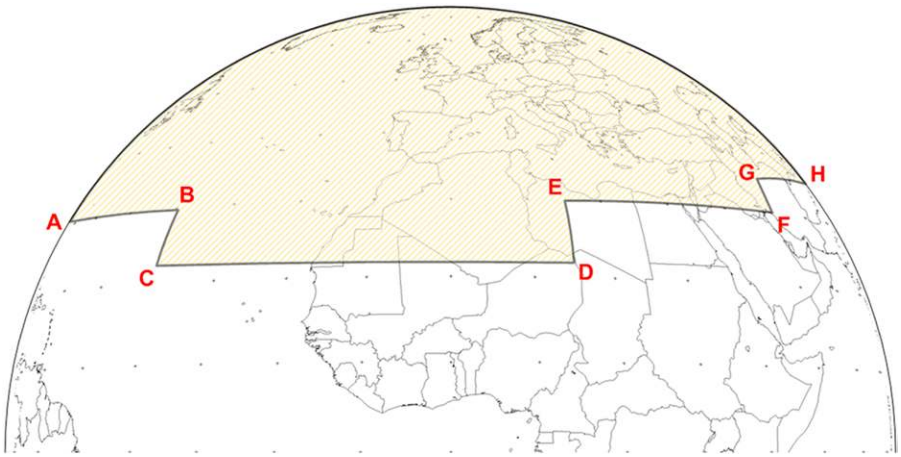

Fig. 5. Mandatory LAC zone 4 coverage for IRS Operational Scenario. The diagram indicates the mandatory LAC zone 4 coverage in terms of latitude and longitude on the Earth. The LAC area is determined by longitude and latitude lines as follows: AB = 30°N, BC =40°W, CD = 22°N, DE = 15°E, EF = 30°N, FG = 50°E, GH = 35°N.

The geophysical products from the IRS available at the

Table 7. The key characteristics of the Infrared Sounder on board MTG.

Spectral band	Status	Wavenumber range	Spectral channel interval	Spatial sampling distance (SSD)
LWIR	Extended	680–700 cm^{-1}	<0.625 cm^{-1}	4.0 km
	Specified	700–1,210 cm^{-1}		
MWIR	Specified	1,600–2,175 cm^{-1}	<0.625 cm^{-1}	4.0 km
	Extended	2,175–2,250 cm^{-1}		

Coverage	Repeat cycle duration	Comment
FDC = 17.70° diameter circle centered at SSP	—	Indicates the maximum coverage achievable by combining four LACs
LAC = FDC/4	15-min dwell/6-h repetitive scan pattern	

start of operations will be profiles of atmospheric temperature, specific humidity, and ozone. In addition, total column water vapor, total column ozone, land/sea surface temperature, and land surface emissivity will be provided. The cloud products include cloud mask, cloud effective coverage, cloud-top pressure, and a dust indicator.

Sentinel-4/UVN: The ultraviolet–visible–near-infrared sounding instrument. The Copernicus Sentinel-4/UVN mission consists of an ultraviolet–visible–near-infrared (UVN) imaging spectrometer instrument embarked on the MTG-S satellite. The main objective of the Sentinel-4/UVN mission is to monitor air quality, trace gases, and aerosols over Europe in support of the Copernicus Atmosphere Monitoring Service (CAMS) at high spatial resolution and with a frequent revisit time. ESA is responsible for the development and provision of the Sentinel-4/UVN Instrument, whereas EUMETSAT takes responsibility for operating the instrument and the operational processing, delivery, and management of the instrument data.

The observations in the UVN band can be strongly polarized. For Sentinel-4/UVN sensitivity to polarization is minimized through the optical design and use of polarization scramblers. The instrument is realized with a single telescope for all spectral bands, followed by a dichroic beam splitter combined with the entrance slit assembly, which separates the near-infrared (NIR) from the ultraviolet–visible (UV-VIS) band(s). The UV-VIS bands (305–500 nm) are covered by a single spectrometer all the way down to the detector, otherwise known as the focal plane assembly (FPA). The NIR spectral band (750–775 nm) is also covered by a single spectrometer and detector or FPA. The spectral resolution is for the UV-VIS ≤ 0.5 nm and for the NIR ≤ 0.12 nm, with a spatial sampling distance of about 8 km. More details on the characteristics of the instrument are given in Table 8.

A subsection of the Earth disk will be measured by repetition of 1-h scans from east to west. Each scan is followed by a rapid 20-s backscan to the starting position in the east. Note that the Sentinel-4/UVN instrument does not observe the full illuminated Earth disk. The instrument only observes the area over Europe and the North Atlantic, as indicated in Fig. 6. The overall daily Earth observation pattern consists of a series of 1-h-long east-to-west scans ("repeat cycles") with a fast west-to-east retrace in between. Depending on the seasonally varying duration of Earth illumination by the sun, the daily Earth observation scan series consist of 16 (winter) to 20 (summer) 1-h scans. The first scan of a day starts at the eastern edge of the geostationary coverage area. The 1-h repeat cycle coverage is shifted westward in two steps during each day in order to follow the sun illumination and to achieve full coverage (Gulde et al. 2017).

The Sentinel-4/UVN measurement concept is based on the observation of backscattered solar light. The observed Earth radiance is strongly dependent on the observation geometry defined between the incident solar irradiance and the radiance backscattered from the Earth

Table 8. Main design and performance parameters of Sentinel-4/UVN.

Spectral			
Parameter	**UV–VIS values**	**NIR values**	**Comments**
Wavelength range	305–500 nm	750–775 nm	
Spectral resolution/spectral oversampling	0.5 nm/>3	0.12 nm/>3	Oversampling is resolution divided by spectral pixel sampling
Spectral calibration accuracy	0.0017 nm	0.0020 nm	
Geometric and temporal coverage			
Parameter	**Value(s)**		**Comments**
Spatial sampling distance (SSD)	8 km (EW) × 8 km (NS)		On-ground-projected SSD at reference point in Europe (45°N latitude; subsatellite-point longitude)
Integrated energy	70% over 1.47 SSD EW × 1.13 SSD NS		Integrated energy is a measure for the spatial resolution of the instrument
	90% over 1.72 SSD EW × 1.72 SSD NS		
N/S slit field-of-view (swath)	4.0°		
East–west coverage and repeat cycle	See Fig. 7		See Fig. 7
Daily Earth observation time [1 Jan 2000 (UTC)]	Summer max: 0140–2140		Adjusted to seasonally varying solar Earth illumination on monthly basis
	Winter min: 0340–1940		
Spatial co-registration	Intra-detector: 10% of SSD		Two-dimensional (E/W and N/S) absolute co-registration
	Inter-detector: 20% of SSD		
Radiometric			
Parameter	**UV-VIS values**	**NIR values**	**Comments**
Optical throughput	~50% (in UV)	~60%	End-to-end scanner-to-detector
Radiometric aperture	70 mm	44 mm	Circular diameter
Earth signal-to-noise ratio (SNR)	UV: >160	759–770 nm: >90	For specified Earth radiance reference scene
	VIS: >1600	Rest NIR: >600	
Earth absolute radiometric accuracy (RA)	<3% (2% goal)	<3% (2% goal)	For Earth radiance and reflectance
Sun absolute radiometric accuracy (RA)	<3% (2% goal)	<3% (2% goal)	For sun irradiance
Polarization sensitivity	<1%	<1%	
Polarization spectral features	<0.015%	<0.1%	Caused by speckle effect
Sun diffuser spectral features	<0.042%	<0.076%	

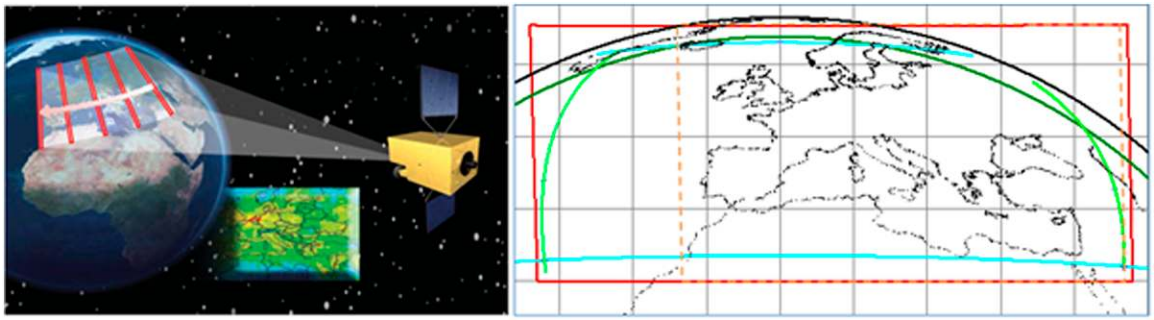

Fig. 6. Earth observation and scan concept of Sentinel-4/UVN. The right-hand picture shows Earth coverage from the geostationary Sentinel-4/UVN perspective. Green/turquoise lines indicate the borders of the specified geostationary coverage area, which is the total area to be covered every day. The red rectangle represents the actual daily observation area covered by multiple east–west scans of the north–south–oriented slit field of view. The orange dashed rectangle indicates the size of a 1-h repeat cycle (reference coverage). Depending on the seasonally varying duration of Earth illumination by the sun, the daily Earth observation scan series consist of 16 (winter) to 20 (summer) 1-h scans (Gulde et al. 2017).

and the atmosphere and received by the Sentinel-4/UVN instrument. The observation geometry strongly varies with the diurnal cycle of sun position, solar zenith angle (SZA). Therefore, the required observation starts in the morning when the scene is illuminated with a SZA less than 92°.

The number of 1-h east–west scans is a function of season, as the illumination conditions over the geographical coverage zone change with season. Typically, the Earth measurements are performed between 0300 and 2100 UTC, but more Earth radiance measurements are performed in the summer than in the winter. During the times when the Sentinel-4/UVN is not measuring Earth radiance, i.e., during the night, several calibration measurements are performed: sun, dark, background, star, sometimes moon, white light source (WLS), and light-emitting diodes (LED). The non-Earth-radiance calibration and characterization measurements have different observation frequencies: daily, weekly, monthly, and incidental. The measurement configurations are organized in measurement sequences.

In addition to the Earth radiance and solar irradiance, which are also distributed to all users, the primary geophysical products are ozone, nitrogen dioxide, sulfur dioxide, formaldehyde, glyoxal, and aerosol and cloud properties. The full list of Level 2 products from the Sentinel-4/UVN instrument available at the start of operations is given in Table 9.

The applications

Nowcasting and very short-range numerical weather prediction. One of the main applications of geostationary satellite data is nowcasting. The main MTG instruments for nowcasting will be FCI, IRS, and LI. The current state of the atmosphere can be analyzed from the satellite data, and the information can be extrapolated 3–6 h ahead using nowcasting tools. Beyond 6 h, short-range NWP (SRNWP), with the potential to describe the mesoscale variability of the atmospheric flow including divergence and convergence patterns, becomes increasingly important. These models can make better use of geostationary satellite data with high temporal refresh cycles, providing, e.g., three-dimensional fields of water vapor and cloud observations. Wind fields associated with atmospheric features such as fronts, mesoscale convective complex, and large convective systems, will be better depicted and rapid evolution of convection can be captured in the convective-scale models (e.g., Saunders et al. 2015). Today new methods, such as artificial intelligence and machine learning schemes that are able to use large amounts of complex data sources, are also being developed offering new opportunities for nowcasting (e.g., Boukabara et al. 2019).

The high-resolution and frequent repeat cycle of the FCI will meet the demands of the increased resolution of limited area SRNWP forecast models. It will provide new information on temporal changes of cloud macro- and microphysics, which are important to capture the fast hydrological processes related to cloud and precipitation formation. Particularly the combined use of observations from FCI, LI, and IRS will enable monitoring of convection from the preconvective clear environment until mature convection and severe weather, which is depicted in Fig. 7. Combination of data from multiple sources, e.g., ground-based radar, will further improve nowcasting and provision of weather-related warnings, as shown by Wapler et al. (2015). The finer resolution of IRS, as compared to IASI, will also increase the probability of capturing cloud-free scenes. Therefore, one can confidently expect that MTG-I and MTG-S will improve on the current performance of nowcasting.

The high frequency of the IRS soundings will provide novel inputs for limited area SRNWP models. Geostationary infrared sounding missions offer good temporal coverage; however, due to the large distance to the observed Earth targets, the effect of diffraction is increased compared to sounding from a low-Earth orbit with an impact on instrument performance (Grandell and Stuhlmann 2007). While this may bring some advantages to the polar-orbiting interferometers, their long repeat cycle (12 h) is inadequate to observe the continuous temporal

Table 9. The day 1 products from Sentinel-4/UVN on MTG with target/goal performances.

Product	Threshold	Goal	Scenario
Ozone total column	4%	3%	SZA < 60° VZA < 60° All clouds
Tropospheric ozone	40%	25%	SZA < 60° VZA < 60° CF < 20%
Tropospheric nitrogen dioxide	Troposphere 1.5×10^{15} molecules cm^{-2} or 50%	Troposphere 1.5×10^{15} molecules cm^{-2} or 30%	SZA < 60° VZA < 60° CF < 20%
Sulfur dioxide	Total column 5.0×10^{16} molecules cm^{-2} or 100%	Total column 3.0×10^{16} molecules cm^{-2} or 60%	SZA < 60° VZA < 60° CF < 20%
Formaldehyde	Total column 1.5×10^{16} molecules cm^{-2} or 100%	Total column 1.5×10^{16} molecules cm^{-2} or 50%	SZA < 60° VZA < 60° CF < 20%
Glyoxal	—	Total column random 1.5×10^{15} molecules cm^{-2}, systematic 2.5×10^{14} molecules cm^{-2} or 50%	SZA < 60° VZA < 60° CF < 20%
Aerosol layer height	1 km	—	SZA < 60° VZA < 60° AOD @760 nm > 0.3 ALH > 1.5 km
Aerosol index	0.5	0.3	SZA < 60° VZA < 60° All-cloud
AOD total column	0.05 or 15%	—	SZA < 60° VZA < 60° Cloud-free Homogeneous
Cloud properties	Cloud fraction 20% Cloud-top height 1 km Cloud optical thickness (albedo) 30%	Cloud fraction 10% Cloud-top height 0.5 km Cloud optical thickness (albedo) 20%	SZA < 60° VZA < 60° COT > 5 CF > 10%
Surface	First bidirectional reflectance factor parameter k: 0.02 ($k \leq 0.03$), 0.01 or 5% ($k > 0.03$)	—	SZA < 60° VZA < 60° Cloud-free Homogeneous

evolution of water vapor structures, and even a constellation of satellites cannot provide the same temporal coverage over mid- and low latitudes as geostationary satellites. Furthermore, the spatial sampling of IRS, with smaller and contiguous pixels compared to the polar sounders (sparse pixels typically at 12-km resolution at nadir), offers unprecedented hyperspectral imaging capabilities of the atmospheric thermodynamics. Therefore, one of the promising avenues is to use IRS data to depict vertically resolved atmospheric motion. This information can either be extracted through 4D-Var analysis schemes via the wind tracing effect (Peubey and McNally 2009) or through tracking of water vapor features at various levels using

similar approaches applied for the derivation of AMVs (Velden 2004).

A further advantage of the IRS for nowcasting will be the detection of lower-level water vapor convergence preceding convection together with the retrieval of vertical temperature profiles. The established products for monitoring atmospheric instability from imagers (Koenig and de Coning 2009) and for convective initiation (Mecikalski et al. 2015) will be complemented by the IRS observations. One can expect that the better vertical resolution of the IRS will improve upon the heritage products from the SEVIRI and continued with FCI.

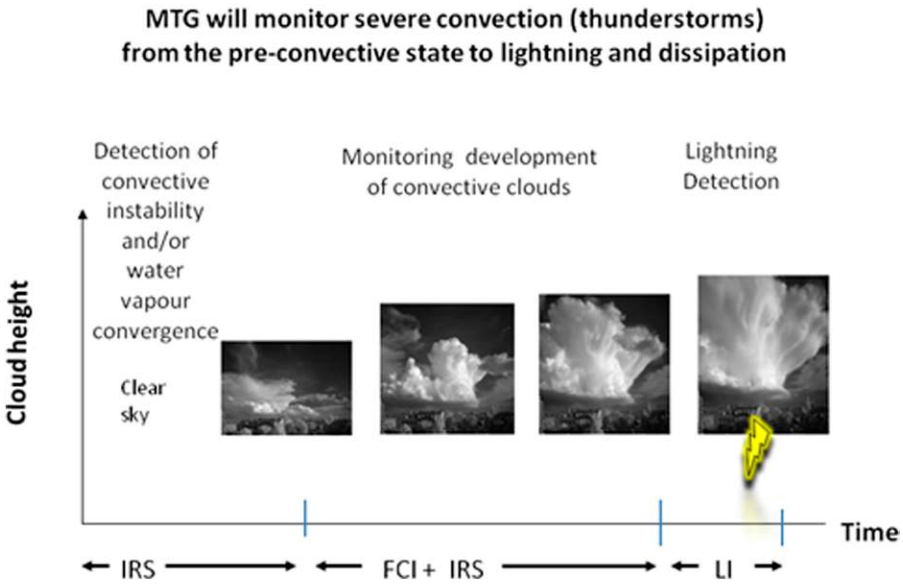

Fig. 7. Sketch of how MTG will observe the life cycle of deep convective clouds and thunderstorms with three of its four instruments.

Thunderstorms and lightning are major natural hazards. They affect transportation, aviation, power grids, wind farms, and forestry and pose a threat on daily life, as every year thousands of people are killed by lightning (Cooray et al. 2007). The applications are therefore wide ranging and information on and prediction of lightning have important practical applications in different parts of society and economy.

The LI mission provides a real-time lightning detection [cloud-to-cloud (CC) and cloud-to-ground (CG)] and location capability in support to nowcasting and very short-range forecasting (VSRF) of severe storm hazards and lightning strike warning. Lightning is strongly correlated with thunderstorms, and very early detection of severe weather and therefore LI data can be used as proxy to describe other characteristics of severe convection such as convective rainfall, hail, or updraft strength. It can also be used as a proxy for adiabatic heating through the release of latent heat. However, in the long run it may appear a good way to include the physics of cloud electrification over and above the cloud microphysics in SRNWP models and develop a pertinent forward operator for the direct use of lightning data in SRNWP models (e.g., MacGorman et al. 2001). Due to the capability to detect total lightning (CC + CG), which has been shown to often provide a lead time for severe weather, LI will also provide the duty forecaster an additional tool for predicting such events to aid the decision-making process for issuing warnings. This becomes particularly interesting in areas where good-quality total lightning information from ground networks is not available. The advance of continuous total lightning observations from geostationary orbit will therefore further improve the ability to monitor and predict thunderstorm development throughout Africa (Virts and Goodman 2020). An interesting development is to use LI measurements in lieu of radar when radar measurements are not available, as demonstrated by Tollefson (2013).

LI information can also be used to provide non-quantitative visualized weather information to the public warnings about potential severe weather.

Global numerical weather prediction. Global NWP models are used to produce short- and medium-range weather forecasts (out to 10–15 days) of the state of the atmosphere. Satellite data have progressively become the predominant source of information assimilated in the

NWP models. MTG will provide continuity for the currently used data and open exciting new opportunities with the new instruments and improved data quality. The most important MTG instruments for global NWP are FCI, IRS, and LI.

Assimilation of clear-sky radiances from geostationary imagery data in NWP started almost 20 years ago (e.g., Köpken et al. 2004). However, NWP assimilation schemes at different weather centers have also been extended to make use of satellite radiances significantly affected by clouds (Stengel et al. 2012). The use of high-frequency observations presents an opportunity to capture information of the atmospheric dynamics, particularly in the extratropical regions. However, in the tropics, but also elsewhere, the use of AMVs remains a key ingredient in the state of the art assimilation schemes. With the improved performance of FCI, it is expected that the AMVs will continue to have a strong positive impact on NWP data assimilation.

The upcoming hyperspectral IR instruments on board geostationary satellites, like IRS, will provide temperature, humidity, and wind information with high temporal and vertical resolution and have huge potential to further improve NWP. The potential of wind tracing with IRS has been investigated in the European Centre for Medium-Range Weather Forecasts (ECMWF) system. Assimilation of humidity-sensitive radiance observations in a 4D-Var framework impacts the wind analysis via adjustments in the mass field of the atmosphere, and via adjustments in the wind field directly. The wind field can be changed to advect humidity to and from other areas, and this process is called wind tracing. Figure 8 shows the short-range forecast impact against conventional wind observations when either AMVs or radiances from the currently available hyperspectral instruments [IASI, Cross-Track Infrared Sounder (CrIS), and Atmospheric Infrared Sounder (AIRS)] are assimilated. Both sources have clear positive impact on wind forecasts. IRS will have excellent temporal resolution compared to the hyperspectral observations from polar-orbiting satellites. Thus, it can be expected that IRS will have strong positive impact on NWP.

Alternative option to get wind information from IRS is to retrieve wind profiles in clear-sky areas by tracking either observed radiance features or moisture features in the retrieved profiles. The so-called 3D winds would then be important information to the NWP models, in addition to AMVs from FCI, with the benefit of improved height assignment compared to traditional AMVs.

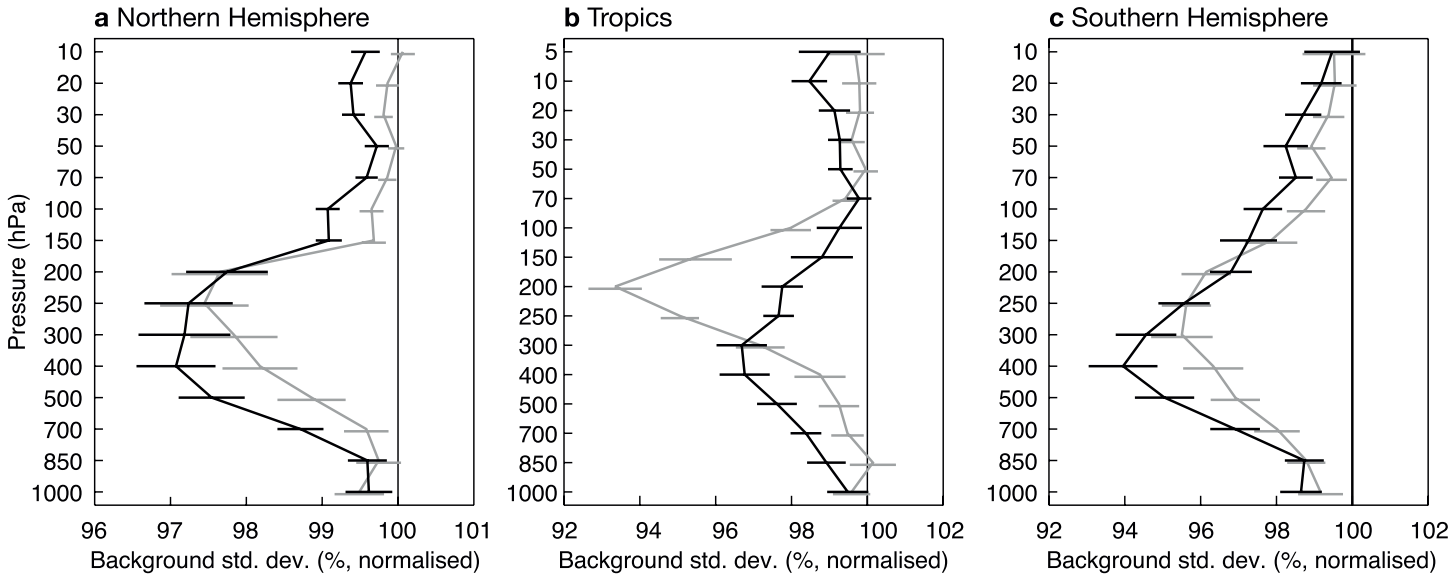

Fig. 8. The improved fit of short-range wind forecasts to independent in situ observations in the (left) Northern Hemisphere, (center) tropics, and (right) Southern Hemisphere, expressed as a percentage reduction of standard deviation. Impact of hyperspectral infrared radiances (black line) is compared to the impact of AMV data (gray line).

An interesting novel application will be the assimilation of cloud-top evolution into numerical models (Wakeling et al. 2014) where MTG cannot only provide cloud-top height changes but also changes in cloud microphysics.

Further benefits for NWP will be provided through the combined use of IRS and LI. While still regional, the IRS and LI data can also be used to improve the determination of atmospheric flow, motion of convective patterns, and cloud evolution. It is furthermore anticipated that the geostationary coverage will continue to improve as other operators like NOAA and CMA continue to deploy similar instruments in the geostationary orbit. Specifically, more can be learned from the *GOES-16* and *GOES-17* GLM and the *FY-4A* LMI and GIIRS, which were launched in November 2016, March 2018, and December 2016, respectively.

The IRS will also provide continuous observations of so-called atmospheric rivers (Zhu and Newell 1998). These are water-vapor-rich parts of the lower troposphere in warm conveyor belts found in extratropical cyclones ("storms"). As the observations can continuously be assimilated into models, improvements in precipitation forecasts could be expected. The improved depiction of water vapor fields in the atmosphere, including vertical segregation, and the temporal resolution from the IRS will provide a basis for breakthroughs in describing fast components of the hydrological cycle such as cloud formation and precipitation.

As for SRNWP, assimilation of lightning information could improve the model cloud physics. One possibility to achieve this would be by nudging the parameterization used to derive lightning from the model data. While initial results are promising (Lopez 2016), significant further work is still required.

Monitoring hazards. Geostationary satellite systems provide opportunity to monitor the Earth system continuously with a high temporal frequency, which is critical for monitoring rapidly changing phenomena like natural hazards. All MTG instruments will provide important observations for these purposes. Some examples are given in the following.

Volcanic eruptions can have a major socioeconomic impact, as shown during the Eyjafjällajökull eruption in 2010, but also pose a potential aviation safety hazard. The continuous monitoring using multispectral techniques as demonstrated by MSG SEVIRI provides important timely information on the extent of volcanic ash clouds as well as a tool for early detection of eruptions. During an explosive volcanic eruption, volcanic ash can be transported to jet cruising altitudes within minutes, underlining the importance of continuous observations. The existing capabilities will be continued with FCI, albeit with improved performance, and further augmented by the Sentinel-4/UVN and IRS data, providing additional capabilities to estimate the volcanic ash cloud height and concentration as well as sulfur dioxide.

Dust outbreaks have strong implications on climate, environment, and human activities. Dust injected into the atmosphere contributes to climate change, impacts human health, and can have an impact on cyclogenesis, e.g., Saharan dust transported to the Atlantic. The MTG instrument suite will also provide new insight into the monitoring of dust and support operational early warning systems.

Most fires are man-made and have a diurnal cycle through agricultural practices, occur in the tropics, are rather small, and have a duration of up to a few hours. Wildfires are a threat to populated regions directly as fire hazard or indirectly through the emission of polluting smoke. While products from polar-orbiting satellites, like Fire Radiative Power (FRP), which is approximately proportional to the biomass combustion rate and thus the smoke emission rate, are generally of higher accuracy, supplementing this information with the geosynchronous data capturing the diurnal cycle is very important. The high temporal coverage from geostationary orbit provides not only the potential for early detection of strong fire events, but also monitoring the evolution and rapid changes in the direction of propagation, critical for on-ground firefighting, as shown by Schmidt (2020) using *GOES-16* data for the Oklahoma

and Kansas fire event on 7 March 2017. To improve the fire detection capabilities from geostationary orbit, the FCI 3.80-μm channel is specifically designed with two radiometric ranges and a resolution down to 1 km. It should also be noted that products like FRP are today used in monitoring and forecasting of the atmospheric composition in atmospheric environmental services, like the European CAMS services (Peuch et al. 2018).

Floods are among the most frequent of natural disasters, affecting millions of people globally. Despite this, only a few techniques exist for the rapid detection and monitoring of flooded land. While in situ methods produce good quality results, they are expensive, a particular concern in the developing world, where the majority of people affected by such flooding events live. Furthermore, during a flooding event, the ground-based infrastructure may be affected, and quality and availability of observations reduced. Polar-orbiting satellites with their diverse instrumentation, like high-resolution imaging and synthetic aperture radar (SAR), provide significant capabilities for flood monitoring. However, in rapidly changing situations more frequent observations are needed. The high-frequency observations provided with the new-generation geostationary imagers, including FCI, increase the probability of cloud-free observations and enable a faster mapping of flooded areas essential for emergency response functions, as shown in Fig. 9 (Goldberg et al. 2018). Hence, while polar-orbiting imagery data are often of higher resolution, the geostationary data may have an advantage. The best result would naturally be achieved through combination of both data sources, as demonstrated by Goldberg et al. (2018).

Atmospheric composition and air quality. Until recently, the only possibility to detect and measure atmospheric composition including trace gases and species relevant to air quality from geostationary orbit was using the data from a selected few channels on the imagers. While the capabilities of the low-Earth-orbit satellites are better, due to regional, diurnal, and rapid developments, which are also driven by local weather, there is a strong need for high-quality and high temporal observations from a geostationary orbit (Lahoz et al. 2012). The main MTG instruments for monitoring atmospheric composition and air quality are Sentinel-4/UVN and IRS, supported by FCI.

Geostationary imagers can detect sulfur dioxide and measure ozone. However, the usefulness of these data is limited to some specific cases. Sulfur dioxide measurements are mainly useful in areas with strong concentrations, like in the case of volcanic eruptions, due to the low sensitivity of the instruments. The benefit is that they do provide continuous observations and the capability to track sulfur dioxide over extended periods of time. In synergy with polar sounders, the sulfur dioxide altitude can be determined with the higher spectral resolution of, e.g., IASI or IASI next generation (NG), and the sulfur dioxide plume trajectory and density can be continuously monitored and better forecasted with FCI observations. The derived ozone data from currently flying geostationary satellites have been used to study atmospheric dynamics, reflecting the relationship between ozone and potential vorticity in the stratosphere, as well as for air quality, primarily as a source function in air quality and ozone prediction models. The ozone observations are also useful for monitoring and forecasting UV radiation at the ground level.

Due to the limitations of the geostationary imagers, it is therefore important to deploy dedicated instruments to monitor atmospheric composition and air quality from the geostationary orbit. MTG provides this capability with the Sentinel-4/UVN instrument. The main objective of the Sentinel-4/UVN mission on board MTG-S is to measure atmospheric composition and to support air quality monitoring and forecasting over Europe with hourly observations. The mission will focus on air quality, with the main data products being ozone, nitrogen dioxide, sulfur dioxide, formaldehyde, and aerosol optical depth. Figure 10 presents an example of the anticipated capabilities for Sentinel-4/UVN to measure nitrogen dioxide.

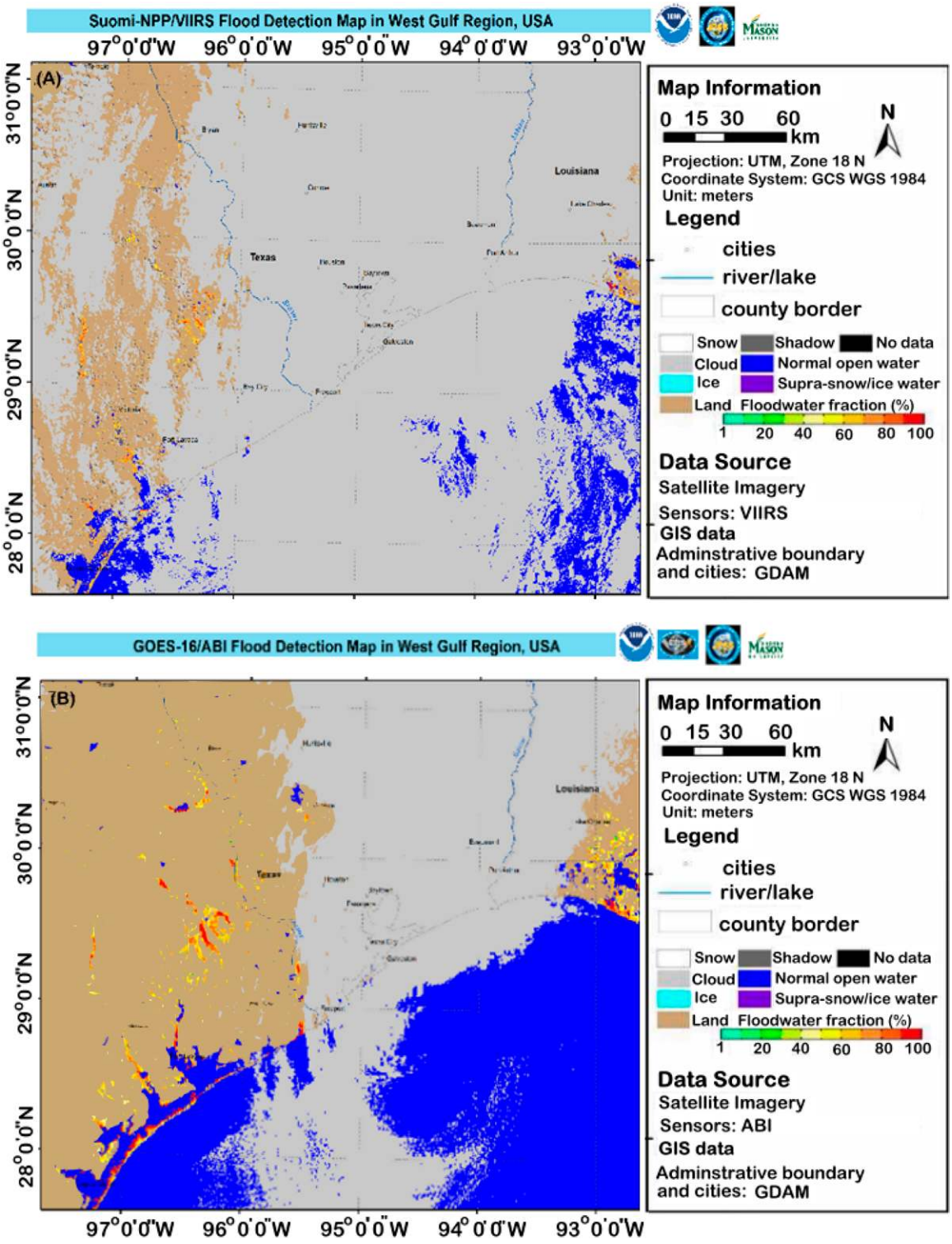

Fig. 9. Flood map from (top) the *Suomi National Polar-Orbiting Partnership* (*SNPP*) satellite Visible Infrared Imaging Radiometer Suite (VIIRS) observations and (bottom) the new *GOES-16* ABI maximum flood extent map composited from 1447 to 1557 UTC 29 Aug 2017 (Goldberg et al. 2018).

The observations by Sentinel-4/UVN are complemented by IRS providing information on ozone, carbon monoxide, and volcanic ash composition. Due to its spectral coverage and spatiotemporal sampling, IRS will be particularly suited to study the diurnal cycle of ammonia, a short-lived species, hence contributing to air quality, anthropogenic point source, and fire monitoring.

Sentinel-4/UVN, together with IRS, will provide a unique, integrated capability to observe ozone, carbon monoxide, sulfur dioxide, and other trace gases, in support of air quality,

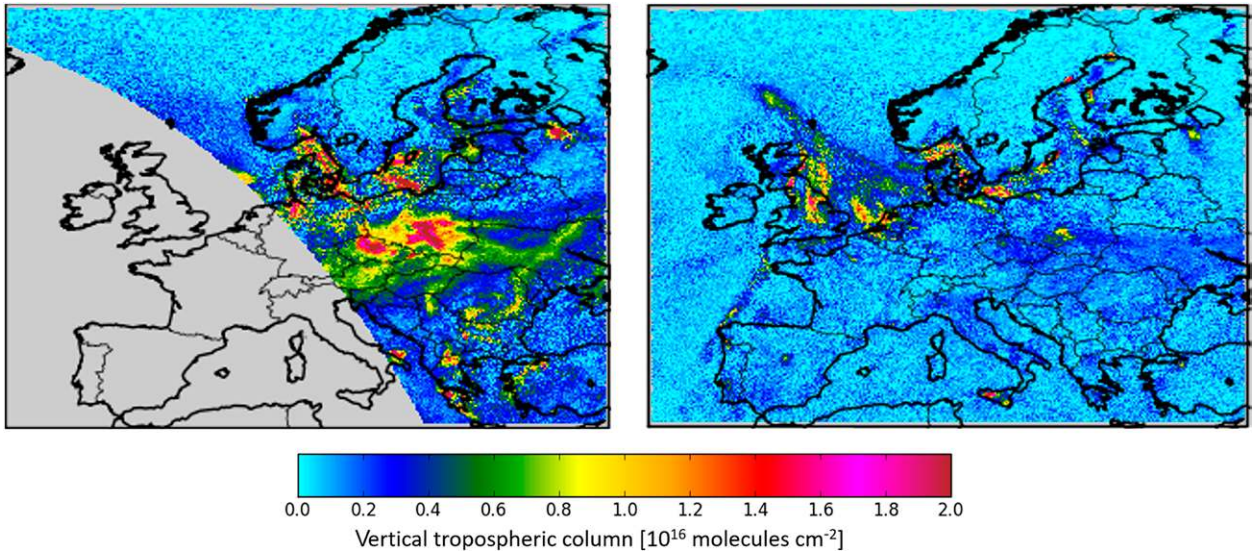

Fig. 10. Example of two Sentinel-4/UVN nitrogen dioxide scenes: early morning at 0400 UTC and midday at 1200 UTC 1 Jun 2003. Data are plotted for solar zenith angles < 85° (Timmermans et al. 2019).

pollution, and climate monitoring. The observations will enable the monitoring of atmospheric composition constituents like tropospheric ozone, aerosols, and their precursors, which are important factors in understanding air quality and climate change. The Committee on Earth Observation Satellites (CEOS) Atmospheric Composition Constellation white paper "A geostationary satellite constellation for observing global air quality: An international path forward" (CEOS 2011) notes: "Ozone, the ozone precursors nitrogen dioxide and carbon monoxide, and aerosols are pollutants that adversely affect human and plant health and the environment." Ozone and aerosols are also the primary short-lived climate forcers, meaning that future air quality and climate are closely linked. Emissions of these pollutants are strongly influenced by human activities. Their distributions in the atmosphere depend on complex physical and chemical transformations that are controlled by sunlight and weather, including the rapidly varying planetary boundary layer and continental- and intercontinental-scale transport of pollution. Understanding and monitoring these processes requires continuous measurements with high temporal and spatial resolution possible only from geostationary Earth orbit. It should, however, be noted that there is still a need to complement these observations with data from geostationary imagers like FCI for better spatial and temporal coverage as well as resolution.

South Korea's Geostationary Environment Monitoring Spectrometer (GEMS) instrument on the Korean Aerospace Research Institute *GEO-KOMPSAT-2B* satellite, which was launched 18 February 2020; NASA's Tropospheric Emissions: Monitoring of Pollution (TEMPO) planned for launch around 2022; and Sentinel-4/UVN will form a constellation that will revolutionize the way scientists observe air quality over a large part of the Northern Hemisphere (Kim et al. 2019).

Finally, it should be noted that there is progress on the modeling side to make use of LI data for atmospheric chemistry. Tost et al. (2007) tested convection and lightning parameterizations in simulations with a global atmospheric chemistry model and evaluated results against lightning observations. They conclude that the sequence of parameterizations of convection and lightning entails very large uncertainties. While it is known that for atmospheric chemistry, lightning plays a significant role in generating nitrogen oxides, the natural nitrogen oxide budget has a high uncertainty. Continuous long-term observations of sources, such as lightning, may therefore prove valuable and novel information.

Climate monitoring. Geostationary satellites also contribute to climate monitoring. Although the previous generations of geostationary satellites were not originally designed for such applications, the careful reprocessing of the data provides valuable information on the variability of climate parameters. One example is surface albedo discussed in Lattanzio et al. (2013), where more than 30 years of observations have been accumulated and reprocessed to provide a unique climate data record. Albedo is a good tool to monitor large-scale changes in vegetation as well as in general land use and can well depict regional changes and differences. It is also, through its direct control of the surface radiation budget, an important input to weather and climate models. Albedo is one of the essential climate variables (ECV) listed by Global Climate Observing System (GCOS) and the requirement for long-term, global, homogeneous, and complete datasets is high. With FCI the geostationary albedo record over Africa and Europe will be continued, with further improvements through the FCI, in particular in terms of calibration and increased capabilities to detect cloud contamination and aerosol. The derivation of global climate products will also benefit from the availability advent of geostationary and polar imagers with very similar capabilities as noted in the "Flexible Combined Imager" section.

There are several key variables that can be used for a wide range of land biosphere applications that are more directly related to vegetation properties and health than conventional empirical indices. Remote sensing techniques employing satellite multispectral data provide an accurate means of detecting, quantifying, mapping, and monitoring change in vegetation on local, regional, and global scales (Rock et al. 1993). The EUMETSAT Satellite Application Facility on Land Surface Analysis (LSA SAF) produces several of those variables, making them available both in near–real time and offline. Changes in the land cover either caused by changes in land use, climate change, or natural hazards (like forest fires or droughts, for instance) may have a huge social and economic impact. Remote sensing provides the best means to monitor changes in vegetation over a wide range of temporal scales over large areas.

Monitoring evapotranspiration and drought and the impact on agricultural is an important component of food and water security. Remote sensing provides valuable opportunities for continent-wide assessment of droughts with high spatial and temporal resolution (Winkler et al. 2017), for example, monitoring the severe droughts that frequently affect eastern Africa, causing crops to shrink and threatening millions of people with starvation.

Agricultural systems are climate sensitive, and conventional surface instrument networks are sparse and sometimes with significant latency, particularly in developing countries. Satellite monitoring therefore provides the potential for global efficient and timely monitoring of water balance and deficits and can be used to supplement coarser-resolution data from weather and precipitation networks to assess drought conditions. While traditionally polar-orbiting satellite data would be used, FCI will provide the potential to support evapotranspiration and water stress modeling as well as vegetation stress monitoring. As signatures of vegetation stress are manifested in the land surface temperature signal, which can be established by the thermal infrared (TIR) window data, a TIR-based drought index can provide an effective early warning of impending agricultural drought.

The advent of improved lightning observations, including space-based observations, now also provide the opportunity to support climate monitoring. Lightning is therefore recognized by GCOS as a new ECV (Aich et al. 2018).

Finally, it should also be noted that the atmospheric composition and air quality information provided by the Sentinel-4/UVN and IRS instruments are also important for climate and will provide new information on the diurnal variation of trace gases and supporting process studies. Through the MTG Programme these observations will continue into the 2040s and will eventually also be used for the derivation of standalone fundamental climate data records (FCDRs).

Marine applications. The well-calibrated and characterized FCI instrument, as well as IRS, is likely to find other applications beyond the common meteorological user community. For instance, Ruddick et al. (2014) illustrate the opportunities provided by current geostationary imagers for ocean monitoring. The high temporal repeat cycle improves the probability of detecting clear areas and it resolves fast ocean processes such as tidal variability of suspended matter and plankton. FCI with its better spatial and temporal resolution and more channels in the solar spectrum is expected to deliver improved ocean observations.

The large-scale behavior of sea surface temperature (SST) is well captured by buoys. Polar-orbiting satellite data, which provide at least four observations per day, satisfy the Nyquist sampling requirements for the description of the general diurnal cycle. Geostationary satellite data increase the probability for cloud-free observations during the day and may provide a more accurate depiction of the diurnal cycle. The high temporal resolution also allows detection and monitoring of cases with rapid changes of the surface conditions like in coastal upwelling events. Accurate SST retrievals also enable the identification of strong surface gradients. These can be exploited for the identification of SST fronts, currents, and eddies. The high temporal coverage with geostationary data, combined with the associated increased probability for cloud-free observations, then give the opportunity to track sea surface structures as shown in Fig. 11 (Legeckis and Le Borgne 2009).

Geostationary meteorological satellites can also be used for ocean color monitoring. While it is difficult to achieve a visible calibration of 1% for ocean color applications, there are some parameters that can be derived with meteorological geostationary imagers applying improved calibrations methods like lunar calibration as provided by the Global Satellite Inter-Calibration System (GSICS). It has indeed been shown that already today MSG SEVIRI can be used to estimate total suspended matter (TSM) concentration, and turbidity. In addition, coccolithophore, a species of marine phytoplankton, can be detected by MSG SEVIRI (Ruddick et al. 2014) and in the future with FCI.

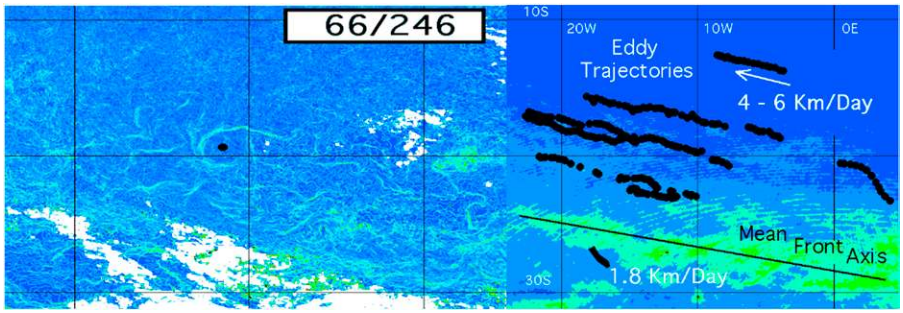

Fig. 11. (left) SST gradients and (right) associated eddy trajectories (Legeckis and Le Borgne 2009).

Additional benefits of MTG

Monitoring the space environment. In recent years, space weather has become an increasing concern. Large-scale geomagnetic storms, like the Carrington event (e.g., Cliver and Dietrich 2013), have the potential to knock out power grids and affect telecommunications. Even smaller-scale events may have an impact, as demonstrated by the solar storm in 2015, which made all airplanes disappear from the Swedish Air Traffic Control System for 90 min. Monitoring the space environment, including conditions in the magnetosphere, ionosphere, thermosphere, and exosphere, is therefore becoming increasingly important. The MTG satellites will carry a radiation monitoring unit (RMU) to monitor the immediate space environment around the platforms, hence also supporting the routine monitoring of the low-Earth-orbit charged particle environment and improving the modeling and understanding of the space environment.

Geostationary Orbiting Search and Rescue (GEOSAR) relay. As with previous Meteosat satellite series, MTG will carry a small communications payload (GEOSAR) to relay distress

signals of 406-MHz beacons to a central reception station in Europe, which passes the signals on for quick organization of rescue activities. The geostationary relay allows a continuous monitoring of the Earth disk and immediate alerting.

Data collection and retransmission. The collection and distribution of environmental data from Data Collection Platforms is one of the core services operated by EUMETSAT in support of Meteorology and Weather Prediction. It is achieved via the Data Collection and Distribution Service (DCS), which provides distribution mechanisms for data transmitted from sensors located on the surface of the Earth and within its atmosphere. The DCS was initially established with the first generation of Meteosat satellites, and has been continued and expanded with MSG. It will be expanded again with MTG with the reserved extended DCP frequency range from 402.43525 to 402.8500 MHz. For further details see EUMETSAT (2018).

Concluding remarks

This article provides a summary of the instruments on board MTG satellites and the committed applications at day 1 of operations. MTG will become the backbone of the European operational meteorological applications for the next two decades, taking over operational services from the current MSG satellites, and is EUMETSAT's contribution toward the geostationary component of the World Meteorological Organization's Integrated Global Observing System Vision 2040 (WMO 2020). The requirements for MTG address nowcasting and very short-term weather forecasting, medium/short-range global and regional numerical weather prediction, climate, and air composition monitoring. These needs will be met by the unprecedented deployment of four instruments on two platforms in geostationary orbit:

1) the Flexible Combined Imager (FCI) covering (i) the Full Disk High Spectral Resolution Imagery (FDHSI) mission and (ii) the High Resolution and Fast Imagery (HRFI),
2) the Lightning Imager (LI),
3) the Infrared Sounder (IRS), and
4) the Ultraviolet–Visible–Near-Infrared sounder Sentinel-4/UVN.

While MTG will seamlessly continue the established services from MSG, it will also enable substantial improvements in terms of continuous monitoring of the atmosphere and will open the door to new applications and services. For instance, the suite of instruments allows observations of convection from the preconvective clear environment to established mature convective system with lightning. The advent of MTG will also pose a challenge for research and development. It is to be expected that the full benefit from the new instruments will only become fully exploited once the data will be available. However, the agreed and committed services at day 1 will already provide novel and useful products and services to the users, especially in the area of quantitative nowcasting applications.

Through the MTG User Preparation Project (MTGUP), EUMETSAT is supporting users and application developers, mainly in European national meteorological and hydrological services, in their preparations for MTG data. The User Preparation Project is engaging users in activities that encompass training, operational testbeds, generation of MTG user familiarization test data, transition to new data access services, and events to exchange knowledge and to raise awareness. The overarching goals of MTGUP are to ensure that (i) meteorological services transition smoothly from using SEVIRI to FCI data, and (ii) services reap operational benefits from the enhancements and innovation offered by MTG (new FCI channels, geostationary lightning data, geostationary hyperspectral IR soundings, UVN soundings for atmospheric composition).

With similar objectives, EUMETSAT is in a close dialogue with users in Africa through the WMO Regional Association I (Africa) Dissemination Expert Group. Through this dialogue and in working with partners in Europe and Africa, EUMETSAT facilitates the provision of operational data access and of training activities. Some areas in Africa (Congo basin, Lake Victoria region) are among the most lightning intense in the world (Virts et al. 2013); hence, geostationary Lightning Imager data from MTG hold significant promise to further operational forecasting and research activities in Africa.

MTG will put European satellite meteorology back to the leading edge of meteorological observations from geostationary satellites. An interesting perspective for the future is also that geostationary imagers operated by other space agencies (NOAA, CMA, JMA, and KMA), and coordinated within the Coordination Group for Meteorological Satellites (CGMS), already have similar capabilities. The commonality in capability will benefit the development of products and applications of geostationary imagery data through intensified international scientific cooperation. In addition, some of the aforementioned agencies will also launch and operate additional new instruments similar to those on MTG, becoming a central element in future international collaboration advancing remote sensing applications using data from geostationary.

MTG will provide societies in Africa and Europe with unprecedented information about severe weather, leading to improved warnings. MTG observations will help people to become more aware of weather risks and to prepare for threats from severe weather. MTG will therefore help to realize the concept of "weather-ready" nations within the Meteosat field of view.

In addition to the products and application areas presented in this paper, the full utilization of the MTG capability will be provided by the EUMETSAT Satellite Application Facility (SAF) Network. For further information on the SAF's products and services, the reader is advised to visit the EUMETSAT web pages: www.eumetsat.int/website/home/Satellites/GroundSegment/Safs/index.html.

Acknowledgments. The authors thank Dr. Martin Setvak, Czech Hydrometeorological Institute, for the depiction of a thunderstorm used in Fig. 7.

References

Aich, V., R. Holzworth, S. J. Goodman, Y. Kuleshov, C. Price, and E. Williams, 2018: Lightning: A new essential climate variable. *Eos, Trans. Amer. Geophys. Union*, **99**, https://doi.org/10.1029/2018EO104583.

Bessho, K., and Coauthors, 2015: An introduction to Himawari-8/9 – Japan's new generation geostationary meteorological satellites. *J. Meteor. Soc. Japan*, **94**, 151–183, https://doi.org/10.2151/jmsj.2016-009.

Boukabara, S. A., V. Krasnopolsky, J. Q. Stewart, E. S. Maddy, N. Shahroudi, and R. N. Hoffman, 2019: Leveraging modern artificial intelligence for remote sensing and NWP: Benefits and challenges. *Bull. Amer. Meteor. Soc.*, **100**, ES473–ES491, https://doi.org/10.1175/BAMS-D-18-0324.1.

CEOS, 2011: A geostationary satellite constellation for observing global air quality: An international path forward. Committee on Earth Observation Satellites, 41 pp., https://ceos.org/observations/documents/AC-VC_Geostationary-Cx-for-Global-AQ-final_Apr2011.pdf.

Cliver, E. W., and W. F. Dietrich, 2013: The 1859 space weather event revisited: Limits of extreme activity. *J. Space Wea. Space Climate*, **3**, A31, https://doi.org/10.1051/swsc/2013053.

Cooray, V., C. Cooray, and C. J. Andrews, 2007: Lightning caused injuries in humans. *J. Electrost.*, **65**, 386–394, https://doi.org/10.1016/j.elstat.2006.09.016.

de Waard, J., W. P. Menzel, and J. Schmetz, 1992: Atlantic data coverage by METEOSAT-3. *Bull. Amer. Meteor. Soc.*, **73**, 977–983, https://doi.org/10.1175/1520-0477(1992)073<0977:ADCB>2.0.CO;2.

EUMETSAT, 2018: TD 16 - Meteosat Data Collection and Distribution Service. Doc. EUM/OPS/DOC/08/0325, 63 pp., www-cdn.eumetsat.int/files/2020-05/pdf_td16_meteosat_data_collection_and_distribution_service.pdf.

Goldberg, M., S. Li, S. Goodman, D. Lindsey, B. Sjoberg, and D. Sun, 2018: Contributions of operational satellites in monitoring the catastrophic floodwaters due to Hurricane Harvey. *Remote Sens.*, **10**, 1256, https://doi.org/10.3390/rs10081256.

Goodman, S. J., and Coauthors, 2012: The *GOES-R* proving ground accelerating user readiness for the next-generation geostationary environmental satellite system. *Bull. Amer. Meteor. Soc.*, **93**, 1029–1040, https://doi.org/10.1175/BAMS-D-11-00175.1.

Grandell, J., and R. Stuhlmann, 2007: Limitations to a geostationary infrared sounder due to diffraction: The Meteosat Third Generation Infrared Sounder (MTG IRS). *J. Atmos. Oceanic Technol.*, **24**, 1740–1749, https://doi.org/10.1175/JTECH2055.1.

——, and Coauthors, 2010: EUMETSAT Meteosat Third Generation (MTG) Lightning Imager: From mission requirements to product development. *2010 Union Fall Meeting*, San Francisco, CA, Amer. Geophys. Union, Abstract AE21A-0257.

Gulde, S. T., M. G. Kolm, D. J. Smith, R. Maurer, G. Bazalgette Courrèges-Lacoste, M. Sallusti, and G. Bagnasco, 2017: Sentinel 4: A geostationary imaging UVN spectrometer for air quality monitoring: status of design, performance and development, *Proc. SPIE*, **10563**, 1056341, https://doi.org/10.1117/12.2304099.

Kim, J., and Coauthors, 2019: New era of air quality monitoring from space: Geostationary Environment Monitoring Spectrometer (GEMS). *Bull. Amer. Meteor. Soc.*, **101**, E1–E22, https://doi.org/10.1175/BAMS-D-18-0013.1.

Klaes, D., and Coauthors, 2007: An introduction to the EUMETSAT polar system. *Bull. Amer. Meteor. Soc.*, **88**, 1085–1096, https://doi.org/10.1175/BAMS-88-7-1085.

Koenig, M., and E. De Coning, 2009: The MSG global instability indices product and its use as a nowcasting tool. *Wea. Forecasting*, **24**, 272–285, https://doi.org/10.1175/2008WAF2222141.1.

Köpken, C., G. Kelly, and J.-N. Thepaut, 2004: Assimilation of Meteosat radiance data within the 4D-Var system at ECMWF: Assimilation experiments and forecast impact. *Quart. J. Roy. Meteor. Soc.*, **130**, 2277–2292, https://doi.org/10.1256/qj.02.230.

Lahoz, W. A., and Coauthors, 2012: Monitoring air quality from space: The case for the geostationary platform. *Bull. Amer. Meteor. Soc.*, **93**, 221–233, https://doi.org/10.1175/BAMS-D-11-00045.1.

Lattanzio, A., and Coauthors, 2013: Land surface albedo from geostationary satellites A multiagency collaboration within SCOPE-CM. *Bull. Amer. Meteor. Soc.*, **94**, 205–214, https://doi.org/10.1175/BAMS-D-11-00230.1.

Legeckis, R., and P. Le Borgne, 2009: EUMETSAT geostationary satellite monitors the sea surface temperatures of the Atlantic and Indian Oceans since 2004. *Environ. Res. Eng. Manage.*, **49** (3), 4–9, https://erem.ktu.lt/index.php/erem/article/view/37.

Lopez, P., 2016: A lightning parameterization for the ECMWF integrated forecasting system. *Mon. Wea. Rev.*, **144**, 3057–3075, https://doi.org/10.1175/MWR-D-16-0026.1.

MacGorman, D., J. M. Straka, and C. L. Ziegler, 2001: A lightning parameterization for numerical cloud models. *J. Appl. Meteor.*, **40**, 459–478, https://doi.org/10.1175/1520-0450(2001)040<0459:ALPFNC>2.0.CO;2.

Mecikalski, J. R., P. D. Watts, and M. Koenig, 2011: Use of Meteosat Second Generation optimal cloud analysis fields for understanding physical attributes of growing cumulus clouds. *Atmos. Res.*, **102**, 175–190, https://doi.org/10.1016/j.atmosres.2011.06.023.

——, J. K. Williams, C. P. Jewett, D. Ahijevych, A. LeRoy, and J. R. Walker, 2015: Probabilistic 0-1-h convective initiation nowcasts that combine geostationary satellite observations and numerical weather prediction model data. *J. Appl. Meteor. Climatol.*, **54**, 1039–1059, https://doi.org/10.1175/JAMC-D-14-0129.1.

Peubey, C., and A. P. McNally, 2009: Characterization of the impact of geostationary clear-sky radiances on wind analyses in a 4D-Var context. *Quart. J. Roy. Meteor. Soc.*, **135**, 1863–1876, https://doi.org/10.1002/qj.500.

Peuch, V.-H., and Coauthors, 2018: The use of satellite data in the Copernicus Atmosphere Monitoring Service (CAMS). *2018 IEEE Int. Geoscience and Remote Sensing Symp.*, Valencia, Spain, 1594–1596, https://doi.org/10.1109/IGARSS.2018.8518698.

Rock, B. N., D. L. Skole, and B. J. Choudhury, 1993: Monitoring vegetation change using satellite data. *Vegetation Dynamics and Global Change*, A. M. Solomon and H. H. Shugart, Eds., Springer, 153–167.

Ruddick, K., G. Neukermans, Q. Vanhellemont, and D. Jolivet, 2014: Challenges and opportunities for geostationary ocean colour remote sensing of regional seas: A review of recent results. *Remote Sens. Environ.*, **146**, 63–76, https://doi.org/10.1016/j.rse.2013.07.039.

Saunders, R., S. Crewell, R. Gelaro, P. J. Minnett, V.-H. Peuch, J. Schmetz, D. Turner, and C. Velden, 2015: Observations for global to convective scale models. *Seamless Prediction of the Earth System: From Minutes to Months*, G Brunet, S Jones, and P. M. Ruti, Eds., WMO 1156, World Meteorological Organization, 15–36, https://library.wmo.int/doc_num.php?explnum_id=3546.

Schmetz, J., P. Pili, S. Tjemkes, D. Just, J. Kerkmann, S. Rota, and A. Ratier, 2002: An introduction to Meteosat Second Generation (MSG). *Bull. Amer. Meteor. Soc.*, **83**, 977–992, https://doi.org/10.1175/BAMS-83-7-Schmetz-2.

Schmidt, C., 2020: Monitoring fires with the GOES-R series. *The GOES-R Series: A New Generation of Geostationary Environmental Satellites*, S. J. Goodman et al., Eds., Elsevier, 145–163.

Schmit, T. J., J. Li, S. A. Ackerman, and J. J. Gurka, 2009: High-spectral- and high-temporal-resolution infrared measurements from geostationary orbit. *J. Atmos. Oceanic Technol.*, **26**, 2273–2292, https://doi.org/10.1175/2009JTECHA1248.1.

——, P. Griffith, M. M. Gunshor, J. M. Daniels, S. J. Goodman, and W. J. Lebair, 2017: A closer look at the ABI on the *GOES-R* series. *Bull. Amer. Meteor. Soc.*, **98**, 681–698, https://doi.org/10.1175/BAMS-D-15-00230.1.

——, S. S. Lindstrom, J. J. Gerth, and M. M. Gunshor, 2018: Applications of the 16 spectral bands on the Advanced Baseline Imager (ABI). *J. Operat. Meteor.*, **6**, 33–46, https://doi.org/10.15191/nwajom.2018.0604.

Stengel, M., M. Lindskog, P. Unden, and N. Gustafsson, 2013: The impact of cloud-affected IR radiances on forecast accuracy of a limited-area NWP model. *Quart. J. Roy. Meteor. Soc.*, **139**, 2081–2096, https://doi.org/10.1002/qj.2102.

Stuhlmann, R., and Coauthors, 2017: Observations depuis l'orbite géostationnaire avec Meteosat troisième génération (MTG). *Meteorologie*, **97**, 52–61, https://doi.org/10.4267/2042/62167.

Timmermans, R., and Coauthors, 2019: Impact of synthetic space-borne NO2 observations from the Sentinel-4 and Sentinel-5P missions on tropospheric NO2 analyses. *Atmos. Chem. Phys.*, **19**, 12 811–12 833, https://doi.org/10.5194/acp-19-12811-2019.

Tollefson, J., 2013: Lightning network tested out in Guinea. *Nature*, **502**, 604–605, https://doi.org/10.1038/502604a.

Tost, H., P. Jöckel, and J. Lelieveld, 2007: Lightning and convection parameterisations – Uncertainties in global modelling. *Atmos. Chem. Phys.*, **7**, 4553–4568, https://doi.org/10.5194/acp-7-4553-2007.

Velden, C., 2004: Environmental satellite data utilization: Determination of wind vectors by sequential moisture analyses derived from hyperspectral IR satellite soundings. *Proc. SPIE*, **5548**, 391–397, https://doi.org/10.1117/12.559955.

Virts, K. S., and S. J. Goodman, 2020: Prolific lightning and thunderstorm initiation over the Lake Victoria basin in East Africa. *Mon. Wea. Rev.*, **148**, 1971–1985, https://doi.org/10.1175/MWR-D-19-0260.1.

——, J. M. Wallace, M. L. Hutchins, and R. H. Holzworth, 2013: Highlights of a new ground-based, hourly global lightning climatology. *Bull. Amer. Meteor. Soc.*, **94**, 1381–1391, https://doi.org/10.1175/BAMS-D-12-00082.1.

Wakeling, M., J. Eyre, S. Hughes, and I. Roulstone, 2014: Assimilation of vertical motion from simulated cloudy satellite imagery in an idealized single column model. *Quart. J. Roy. Meteor. Soc.*, **141**, 1198–1207, https://doi.org/10.1002/qj.2427.

Wapler, K., F. Harnisch, T. Pardowitz, and F. Senf, 2015: Characterisation and predictability of a strong and a weak forcing severe convective event – A multi-data approach. *Meteor. Z.*, **24**, 393–410, https://doi.org/10.1127/metz/2015/0625.

Warner, J. X., R. R. Dickerson, Z. Wei, L. L. Strow, Y. Wang, and Q. Liang, 2017: Increased atmospheric ammonia over the world's major agricultural areas detected from space. *Geophys. Res. Lett.*, **44**, 2875–2884, https://doi.org/10.1002/2016GL072305.

Winkler, K., U. Gessner, and V. Hochschild, 2017: Identifying droughts affecting agriculture in Africa based on remote sensing time series between 2000–2016: Rainfall anomalies and vegetation condition in the context of ENSO. *Remote Sens.*, **9**, 831, https://doi.org/10.3390/rs9080831.

WMO, 2020: Vision for the WMO integrated global observing system in 2040. WMO-1243, 38 pp., https://library.wmo.int/doc_num.php?explnum_id=10278.

Yang, J., Z. Zhang, C. Wei, F. Lu, and Q. Guo, 2017: Introducing the new generation of Chinese geostationary weather satellites, Fengyun-4. *Bull. Amer. Meteor. Soc.*, **98**, 1637–1658, https://doi.org/10.1175/BAMS-D-16-0065.1.

Zhu, Y., and R. E. Newell, 1998: A proposed algorithm for moisture fluxes from atmospheric rivers. *Mon. Wea. Rev.*, **126**, 725–735, https://doi.org/10.1175/1520-0493(1998)126<0725:APAFMF>2.0.CO;2.